2022 IEEE Conference on Control Technology and Applications (CCTA)
August 22-25, 2022. Trieste, Italy

Nonlinear Adaptive Control of Fluid Flow Dynamic Systems Under Actuator Uncertainty

Anu Kossery Jayaprakash[1] and William MacKunis[2]

***Abstract*— A Lyapunov-based adaptive control law is applied to a reduced-order model for a fluid flow dynamic system, which contains parametric uncertainty in both the plant dynamic model and the actuator model. The reduced-order model is derived using a proper orthogonal decomposition (POD) technique. To generate a control-oriented reduced-order model for the actuated flow dynamics, the POD decomposition is performed using both actuated and unactuated modes. This results in a reduced-order flow dynamic model that is in a non-standard mathematical form. This challenge is mitigated through innovative algebraic manipulation in the regulation error system development along with a Lyapunov-based adaptive control law. To the best of the authors' knowledge, this is the first result to apply a nonlinear, Lyapunov-based adaptive control law to the complete actuated POD-based reduced-order flow dynamics to formally compensate for input-multiplicative parametric uncertainty. To achieve the result, a rigorous error system development is presented along with a Lyapunov-based stability analysis. To complement the theoretical development, detailed numerical simulation results are also provided, which show the control design trade-off between the adaptive control law and a standard non-adaptive control law.**

***Index Terms*— Adaptive Control, Nonlinear Control, Lyapunov Analysis**

I. Introduction

Reliable control of fluid flow dynamic systems is critical in a wide range of engineering applications including combustion, turbo machinery, automotive systems, and aeronautics. The potential benefits include aerodynamic drag reduction [1], aeroacoustic noise reduction [2], and lift enhancement in aircraft [3]. While passive and open loop active flow control methods are adequate for many applications, there remain several open problems in the design of reliable closed-loop active flow control systems.

A. Literature Survey

Experimental investigations of AFC systems have been widely presented in recent research [4]–[8]. Applications addressed in these experimental AFC studies include thermal protection [5]; control of vortex-body interaction and wing-tip-vortex meandering in NACA0012 airfoils [4]; low-pressure gas turbines [6]; pressure, force, and moment manipulation in airfoils without moving control surfaces [7]; and flow separation control for performance enhancement in aircraft rudders [8]. Although all of the aforementioned studies have shown promising results in their respective objectives, most of them do not utilize rigorous mathematical tools to model the flow field dynamics and theoretically predict and analyze the influence of AFC on the flow. Dynamic modeling and mathematical analytical techniques can be leveraged to reduce the number of required repetitions and, hence, the time and cost that can be involved in numerical and experimental methods.

To address the challenge of model uncertainty, various linear, robust, and intelligent methods for closed-loop AFC have been presented in recent research literature [9]–[13]. The techniques utilized in these recently developed flow control systems include sliding mode control [9], H_∞-based control [10] and PI control [11]. While methods such as these have been widely shown to achieve promising results in their respective objectives, adaptive control approaches are less popularly utilized in flow control applications.

The use of a standard Lyapunov-based robust and adaptive control system in this result is motivated by the desire to achieve reliable control using a relatively light computational requirement. This is in contrast to time consuming and computationally heavy methods such as machine learning, reinforcement learning, and Q-learning, for example [14]–[16]. While the aforementioned intelligent control approaches have yielded impressive results, the rigorous reduced-order dynamic modeling and active flow control design approach presented here can be implemented in real time, without the need for offline learning or training phases. Further, using this relatively simplistic design approach, the computation time for the resulting control systems can be significantly reduced. This is in stark contrast to reinforcement learning algorithms, for example, in which the computation time can scale polynomially [17] or even exponentially [18] with the number of states [19]. Although the Lyapunov-based robust and adaptive nonlinear control approach described in this paper is nothing new theoretically, the *application* of methods such as these to the *closed-loop fluid flow regulation objective* has rarely been reported in controls literature.

Recent research on adaptive control methods are detailed in [12], [13], [20]–[22], where [12] and [13] specifically discuss the adaptive methods of closed-loop AFC. The strategy

[1]Anu Kossery Jayaprakash*, Ph.D candidate, Physical Sciences Department, Embry Riddle Aeronautical University, Daytona Beach, FL 32114. kosserya@my.erau.edu

[2]William MacKunis, Associate Professor, Physical Sciences Department, Embry Riddle Aeronautical University, Daytona Beach, FL 32114. mackuniw@erau.edu

2022 IEEE Conference on Control Technology and Applications (CCTA) | 978-1-6654-7338-5/22/$31.00 ©2022 IEEE | DOI: 10.1109/CCTA49430.2022.9966108

Authorized licensed use limited to: Embry-Riddle Aeronautical University. Downloaded on December 27,2022 at 18:13:17 UTC from IEEE Xplore. Restrictions apply.

in [12] combines an adaptive controller with an extremum-seeking technique to determine the actuation frequency and forcing amplitude, respectively, for flow separation control over an airfoil. A prediction error-based adaptive control architecture is developed in [13], which utilizes Van der Pol modelling of coupled shear layer von Karman instabilities over a wing section. The adaptive flow control approaches in [12] and [13] demonstrate promising results; however, they do not address the challenge of uncertain actuator dynamics. The current result focuses on developing an **adaptive controller for a POD-based reduced-order flow dynamic model, which includes the complete nonlinear model of both the flow dynamics and the actuator dynamics**.

B. Contribution

In this paper, a Lyapunov-based adaptive controller is presented, which is rigorously proven to achieve asymptotic velocity regulation of a fluid flow field. To the best of the authors' knowledge, this is the first closed-loop active nonlinear AFC result to prove asymptotic flow field regulation using the full nonlinear POD-based reduced-order model, including the complete actuated flow dynamics in addition to input-multiplicative parametric uncertainty.

II. Dynamic Model and Properties

In this section, a POD-based model-order reduction technique is utilized to derive a reduced-order, control-oriented model for the actuated flow dynamics.

A. Reduced-order Model for Flow Field Dynamics

The incompressible Navier-Stokes equations are given as [23]

$$\nabla \cdot u = 0, \qquad \frac{\partial u}{\partial t} = -(u \cdot \nabla)u + v\nabla^2(u) - \nabla p, \tag{1}$$

where $u(s,t) : \mathcal{D} \times [0,\infty) \in \mathbb{R}^3$ denotes the velocity of the flow field over a spatial domain $s \in \mathcal{D} \subset \mathbb{R}^3$; $p(s,t) \in \mathbb{R}^3$ is the space- and time-dependent pressure of the flow field over $\mathcal{D}$; and $v \triangleq 1/\text{Re}$, where Re denotes the Reynolds number.

Proper orthogonal decomposition (POD) expansion, or principal component analysis, is used to obtain lower-dimensional dynamic models for fluid flow. In the POD modal decomposition technique, the flow velocity field $u(s,t)$ is expanded as a weighted sum of actuated and unactuated POD modes defined in the spatial domain $\mathcal{D}$. The actuation effects are embedded in the coefficients of the Galerkin system. Specifically, the actuation effects can be included in the reduced-order model by defining the modal decomposition as [9]

$$u(s,t) = u_0 + \sum_{i=1}^{n} x_i(t)\phi_i(s) + \sum_{i=1}^{m} \gamma_i(t)\psi_i(s). \tag{2}$$

In (2), $\phi_i(s) \in \mathbb{R}^3$ are the POD modes; $x_i(t)$, $i = 1,...,n$, denote unknown, time-varying coefficients resulting from the modal decomposition; $u_0 \in \mathbb{R}^3$ denotes the mean flow velocity over $\mathcal{D}$; $\psi_i(s) \in \mathbb{R}$ denote the actuation modes; and $\gamma_i(t) \in \mathbb{R}$ denote actuation values (i.e., control inputs). By leveraging an input separation method similar to that in [24], the actuation modes can be defined as the modes that minimize the energy not captured in the modal expansion of the actuated flow field.

By substituting the decomposition in (2) into (1), the complete actuated POD-based reduced-order model is obtained as

$$\begin{aligned} \dot{x}_k &= \mathcal{A}_k + \sum_{i=1}^{n} \mathcal{B}_{ki} x_i(t) + \sum_{i=1}^{n}\sum_{j=1}^{n} \mathcal{C}_{kij} x_i(t) x_j(t) \\ &\quad + \sum_{i=1}^{m} \mathcal{D}_{ki}\dot{\gamma}_i(t) + \sum_{i=1}^{n}\sum_{j=1}^{m} \mathcal{E}_{kij} x_i(t)\gamma_j(t) \\ &\quad + \sum_{i=1}^{m} \mathcal{F}_{ki}\gamma_i(t) + \sum_{i=1}^{m}\sum_{j=1}^{m} \mathcal{G}_{kij}\gamma_i(t)\gamma_j(t) \end{aligned} \tag{3}$$

for $k = 1,...,n$. In (3), $\mathcal{A}_k$, $\mathcal{B}_k$, $\mathcal{C}_k$, $\mathcal{D}_k$, $\mathcal{E}_k$, $\mathcal{F}_k$, and $\mathcal{G}_k$ represent constant uncertain scalars, vectors, and matrices of appropriate dimensions, which can be explicitly computed for any given set of numerical or experimental flow field data. Also in (3), $\dot{\gamma}_i(t)$, for $i = 1,...,m$, represents the control input, which can be physically interpreted as a controllable perturbation to the flow field.

Property 1. *Since the fluid flow velocity $u(s,t)$ is based only on physical data collected from high-fidelity computational fluid dynamics (CFD) simulations or experiment, the decomposition in (2) can be used to prove that $\gamma(t)$ is bounded provided $x(t)$ is bounded.*

Remark 1. *The POD-based reduced-order flow dynamic model in (3) is obtained from data collected under a single, fixed set of flow field conditions. Thus, to achieve reliable control of a flow field under realistic uncertain conditions, compensation for parametric uncertainty is of crucial importance for closed-loop flow control applications.*

B. Control-oriented Flow Dynamic Model

After substituting the POD-based modal decomposition in (2) into (1), the reduced-order dynamic model for the actuated flow can be expressed in compact form as

$$\dot{x} = f(x(t), \gamma(t), \theta_1) + \Omega\dot{\gamma} \tag{4}$$

where $f(.)$ denotes a nonlinear (quadratic) auxiliary function, and $\dot{\gamma}(t) \in \mathbb{R}^m$ is introduced in (3). In (4), $\theta_1 \in \mathbb{R}^{p_1}$ denotes a vector of uncertain parameters, and $\Omega \in \mathbb{R}^{m\times m}$ represents an uncertain input gain matrix. Explicit expressions for θ_1 and Ω can be readily obtained from (3).

To facilitate the adaptive control design, the expression in (4) will be rewritten as

$$\begin{aligned} \dot{x} &= \Big(f(x(t), \gamma(t), \theta_1) - f(x_d(t), \gamma(t), \theta_1)\Big) + \Omega\dot{\gamma} \\ &\quad + f(x_d(t), \gamma(t), \theta_1). \end{aligned} \tag{5}$$

Authorized licensed use limited to: Embry-Riddle Aeronautical University. Downloaded on December 27,2022 at 18:13:17 UTC from IEEE Xplore. Restrictions apply.

III. Control Objective and Open Loop Error System

The control objective is to design the control signal $\dot{\gamma}(t)$ to regulate the state vector to a desired reference state. To quantify this objective, a tracking error, denoted by $e(t) \in \mathbb{R}^n$, is defined as

$$e(t) = x(t) - x_d(t) \tag{6}$$

where $x_d(t) \in \mathbb{R}^n$ denotes a desired reference state. The desired state can be defined based on the specific physical control objective at hand (e.g., flow separation control, turbulence reduction, cavity flow control). Based on (6), the control objective can be mathematically stated as

$$e(t) \to 0. \tag{7}$$

Assumption 1. *The desired flow field velocity profile $x_d(t)$ and is bounded and smooth in the sense that*

$$x_d(t) \le \zeta_1, \qquad \dot{x}_d(t) \le \zeta_2 \tag{8}$$

where $\zeta_1,\ \zeta_2 \in \mathbb{R}^+$ are known bounding constants.

A. Open Loop Error System

The open loop dynamics can be developed by taking the time derivative of (6) and using (5) as

$$\begin{aligned}\dot{e}(t) &= \Big(f(x(t),\gamma(t),\theta_1) - f(x_d(t),\gamma(t),\theta_1)\Big) + \Omega\dot{\gamma} \\ &\quad + f(x_d(t),\gamma(t),\theta_1) - \dot{x}_d(t).\end{aligned} \tag{9}$$

To facilitate the subsequent control design and stability analysis, the open loop dynamics can be rewritten as

$$\dot{e}(t) = \tilde{N} + Y_{1d}\theta_1 + Y_2\theta_2 - \dot{x}_d(t) \tag{10}$$

where the auxiliary function $\tilde{N}(x, x_d, \gamma, \theta_1) \in \mathbb{R}^n$ is explicitly defined as

$$\tilde{N} \triangleq f(x(t),\gamma(t),\theta_1) - f(x_d(t),\gamma(t),\theta_1). \tag{11}$$

In (10), $Y_{1d}(x(t),\gamma(t)) \in \mathbb{R}^{n\times p_1}$ and $Y_2(\dot{\gamma}(t)) \in \mathbb{R}^{n\times p_2}$ are measurable regression matrices; and $\theta_2 \in \mathbb{R}^{p_2}$ is a vector of uncertain constants, which are defined via the parameterizations

$$Y_{1d}\theta_1 \triangleq f(x_d(t),\gamma(t),\theta_1); \quad Y_2\theta_2 \triangleq \Omega\dot{\gamma} \tag{12}$$

where the uncertain parameter vector θ_1 is introduced in (4). Note that the uncertain parameter vector θ_2 simply contains the elements of the input-multiplicative vector Ω.

One of the control design challenges for the open-loop system in (4) is that the control input $\dot{\gamma}(t)$ is pre-multiplied by an uncertain matrix. To address this challenge, an estimate of the uncertain matrix Ω, denoted by $\hat{\Omega}(t) \in \mathbb{R}^{m\times m}$, is defined via

$$\hat{\Omega}\dot{\gamma} = Y_2\hat{\theta}_2 \tag{13}$$

where $\hat{\theta}_2(t) \in \mathbb{R}^{p_2}$ is a subsequently defined adaptive estimate of the uncertain matrix Ω (i.e., $\hat{\theta}_2(t)$ contains the elements of $\hat{\Omega}(t)$). Based on (12) and (13), $\Omega\dot{\gamma}$ can be expressed as

$$\Omega\dot{\gamma} = Y_2\tilde{\theta}_2 + \hat{\Omega}\dot{\gamma} \tag{14}$$

where the parameter estimate mismatch $\tilde{\theta}_2(t) \in \mathbb{R}^{p_2}$ is defined as

$$\tilde{\theta}_2 \triangleq \theta_2 - \hat{\theta}_2. \tag{15}$$

The open loop dynamics can be rewritten by substituting (14) into (9) as

$$\dot{e}(t) = \tilde{N} + Y_{1d}\theta_1 + Y_2\tilde{\theta}_2 + \hat{\Omega}\dot{\gamma} - \dot{x}_d(t). \tag{16}$$

Remark 2. *A standard projection algorithm is used to ensure that the parameter estimate matrix $\hat{\Omega}(t)$ remains nonsingular throughout closed-loop controller operation.*

Remark 3. ***(Bounding of $\tilde{N}$)*** *Note that, since $f(x(t),\gamma(t),\theta_1)$ is continuous and differentiable in $x(t)$, the following can be obtained from the mean value theorem:*

$$f(x(t),\gamma(t),\theta_1) - f(x_d(t),\gamma(t),\theta_1) = c_0(x - x_d) = c_0 e(t) \tag{17}$$

where c_0 is a constant. Thus, the definition in (11) can be utilized to upper bound $\tilde{N}$ as

$$\tilde{N} \le c_1 \|e(t)\| \tag{18}$$

where $c_1 \in \mathbb{R}^+$ is a known bounding constant.

IV. Control Design and Closed-loop Error System

The contribution of this paper is development, which shows how a Lyapunov-based adaptive control technique can be applied to achieve asymptotic tracking of a desired fluid flow velocity field in the presence of parametric uncertainty in reduced-order fluid flow dynamic systems in the form given in (3).

Based on the open loop dynamics in (16) and the subsequent stability analysis, the control input is designed as

$$\dot{\gamma} = \hat{\Omega}^{-1}(-Y_{1d}\hat{\theta}_1 - k_1 sgn(e) - k_2 e) \tag{19}$$

where $k_1, k_2 \in \mathbb{R}$ denote positive constant control gains.

Remark 4. *It should be noted that the implemented control law for $\gamma(t)$ given via (20) can be obtained by integrating both sides of the expression. Thus, the actual control law is based on the integral signum, which is continuous in the sense that the time derivative $\dot{\gamma}(t)$ exists and is bounded. This integral signum structure is philosophically motivated by the desire to reduce chattering (or shake) in implementation. Further, since the signum function is not implementable in practice, controllers are usually designed based on low-pass filtered versions of the discontinuous signum function (e.g., the $tanh$ function). To test a practical scenario in this result, the subsequent simulation results utilize the $tanh$ function as an approximation of the signum.*

The closed-loop tracking error system can be developed by substituting the control law (19) into (16) as follows:

Authorized licensed use limited to: Embry-Riddle Aeronautical University. Downloaded on December 27,2022 at 18:13:17 UTC from IEEE Xplore. Restrictions apply.

$$\dot{e} = \tilde{N} + Y_{1d}\theta_1 + Y_2\tilde{\theta}_2 + \hat{\Omega}(\hat{\Omega}^{-1}(-Y_{1d}\hat{\theta}_1 - k_1\,\mathrm{sgn}(e) - k_2 e)) - \dot{x}_d \quad (20)$$

$$\dot{e} = \tilde{N} + Y_{1d}\theta_1 + Y_2\tilde{\theta}_2 - Y_{1d}\hat{\theta}_1 - k_1\,\mathrm{sgn}(e) - k_2 e - \dot{x}_d \quad (21)$$

$$\dot{e} = \tilde{N} + Y_{1d}\tilde{\theta}_1 + Y_2\tilde{\theta}_2 - k_1\,\mathrm{sgn}(e) - k_2 e - \dot{x}_d \quad (22)$$

where the parameter estimate mismatch $\tilde{\theta}_1(t) \in \mathbb{R}^{p_1}$ is defined as

$$\tilde{\theta}_1 \triangleq \theta_1 - \hat{\theta}_1. \quad (23)$$

Based on the closed-loop error system in (22) and the subsequent Lyapunov-based stability analysis, the parameter estimates $\hat{\theta}_1(t)$ and $\hat{\theta}_2(t)$ are generated online according to the adaptive update laws

$$\dot{\hat{\theta}}_1 = \Gamma_1 {Y_{1d}}^T e \quad (24)$$

$$\dot{\hat{\theta}}_2 = \Gamma_2 {Y_2}^T e \quad (25)$$

where $\Gamma_1 \in \mathbb{R}^{p_1 \times p_1}$ and $\Gamma_2 \in \mathbb{R}^{p_2 \times p_2}$ denote diagonal, positive definite adaptation gain matrices.

To facilitate the following stability analysis, the control gains k_1 and k_2 in (22) are selected to satisfy the sufficient gain conditions

$$k_1 > c_1, \qquad k_2 > \zeta_2 \quad (26)$$

where c_1 is introduced in introduced in (18), and ζ_2 is introduced in (8).

V. Stability Analysis

Theorem 1: The adaptive control law described by Equations (19), (24), and (25) achieves asymptotic tracking of a desired flow field velocity in the sense that $e(t) \to 0$, provided the control gain conditions in (26) are satisfied. *Proof:* Consider a non-negative function (i.e., a Lyapunov function candidate) defined as

$$V = \frac{1}{2}e^T e + \frac{1}{2}\tilde{\theta}_1^T \Gamma_1^{-1}\tilde{\theta}_1 + \frac{1}{2}\tilde{\theta}_2^T \Gamma_2^{-1}\tilde{\theta}_2. \quad (27)$$

After taking the time derivative of $V(t)$ along trajectories of the closed loop error system in (22), $\dot{V}(t)$ can be expressed as

$$\dot{V} = e^T(\tilde{N} + Y_{1d}\tilde{\theta}_1 + Y_2\tilde{\theta}_2 - k_1\,\mathrm{sgn}(e) - k_2 e - \dot{x}_d) - \tilde{\theta}_1^T\Gamma_1^{-1}\dot{\hat{\theta}}_1 - \tilde{\theta}_2^T\Gamma_2^{-1}\dot{\hat{\theta}}_2 \quad (28)$$

By substituting the adaptive laws in (24) and (25) into (29) and cancelling common terms, $\dot{V}(t)$ can be rewritten as follows:

$$\dot{V} = e^T(\tilde{N} + Y_{1d}\tilde{\theta}_1 + Y_2\tilde{\theta}_2 - k_1\,\mathrm{sgn}(e) - k_2 e - \dot{x}_d) - \tilde{\theta}_1^T\Gamma_1^{-1}(\Gamma_1 {Y_{1d}}^T e) - \tilde{\theta}_2^T\Gamma_2^{-1}(\Gamma_2 {Y_2}^T e). \quad (29)$$

$$\dot{V} = e^T\tilde{N} - e^T k_1\,\mathrm{sgn}(e) - e^T k_2 e - e^T\dot{x}_d. \quad (30)$$

Based on the bounding inequalities in (8) and (18), $\dot{V}(t)$ can be upper bounded as

$$\dot{V} \leq -(k_2 - c_1)\|e\|^2 - (k_1 - \zeta_2)\|e\|. \quad (31)$$

After using the gain conditions in (26), the upper bound on $\dot{V}(t)$ can be expressed as

$$\dot{V} \leq -\lambda\|e\|^2. \quad (32)$$

where $\lambda \in \mathbb{R}^+$ is a known bounding constant.

Based on (27) and (32), $\tilde{\theta}_1(t)$ and $\tilde{\theta}_2(t) \in L_\infty$ and $e(t) \in L_\infty$. Given that $e(t) \in L_\infty$, (18) can be used to conclude that $\tilde{N} \in L_\infty$. Since $e(t) \in L_\infty$, the assumption that $x_d(t)$ is bounded can be used along with equation (6) to show that $x(t) \in L_\infty$. Given that $x(t) \in L_\infty$, Property 1 can be used to show that $\gamma(t) \in L_\infty$. Since $\gamma(t) \in L_\infty$, the assumption that $x_d(t)$ is bounded can be used along with Equation (12) to show that $Y_{1d}(x, \gamma, \theta_1) \in L_\infty$. Given that $\tilde{\theta}_2(t) \in L_\infty$, Equation (15) can be used to prove that $\hat{\theta}_2(t) \in L_\infty$. Since $\hat{\theta}_2(t) \in L_\infty$, (14) can be used to prove that $\hat{\Omega} \in L_\infty$. Since $\hat{\Omega} \in L_\infty$, the assumption that $\hat{\Omega}$ remains nonsingular can be used to show that $\hat{\Omega}^{-1} \in L_\infty$. Since θ_1 contains bounded system parameters, the fact that $\tilde{\theta}_1(t) \in L_\infty$ can be used along with equation (23) to prove that $\hat{\theta}_1(t) \in L_\infty$. Given that $\hat{\Omega}^{-1}, Y_{1d}(x, \gamma, \theta_1), \hat{\theta}_1(t), e(t) \in L_\infty$, Equation (19) can be used to show that $\dot{\gamma}(t) \in L_\infty$. Since $\Omega, \dot{\gamma} \in L_\infty$, Equation (12) can be used to show that $Y_2(\dot{\gamma}) \in L_\infty$. Since, $\tilde{N}, \tilde{\theta}_1(t)$, $\tilde{\theta}_2(t), Y_{1d}(x, \gamma), Y_2(\dot{\gamma}), e(t) \in L_\infty$, Equation (22) can be used to conclude that $\dot{e}(t) \in L_\infty$, thus $e(t)$ is uniformly continuous. Barbalat's lemma can now be invoked to prove that $e(t) \to 0$ as $t \to \infty$.

VI. Simulation

A numerical simulation was created to test the performance of the proposed adaptive controller. The simulation demonstrates the performance of the control law in (19) using the proposed adaptive law design in (24) and (25). The objective of the simulation is to regulate the flow field velocity to a desired constant value. The objective of regulating the flow field velocity to a constant value is presented as a proof-of-concept only. The proposed closed-loop control method could be applied to drive the flow field to a desired time-varying velocity profile with little modification. The simulation demonstrates the capability of the proposed closed-loop adaptive flow control method to effectively compensate for the parametric uncertainty in the plant dynamic model and actuator model. The reduced-order flow dynamic model in the simulation uses four POD modes, but the proposed control design can be applied to ROM consisting of an arbitrary number of modes.

For completeness in defining the simulation plant model, the values of the constant parameters b_i, L_{ij}, Q_{ijk} for $i, j, k = 1, ..., 4$ are provided in Table II and were taken from (Gordeyev, 2013). The initial conditions of the states and estimates are provided in Table I, and the control gains are are as follows: Γ_1 = 0.0001 × eye(24), Γ_2 = 0.005 × eye(4), k_1 = diag (400;800;800;800) and k_2 = diag (100;300;350;350).

Authorized licensed use limited to: Embry-Riddle Aeronautical University. Downloaded on December 27,2022 at 18:13:17 UTC from IEEE Xplore. Restrictions apply.

The flow field dynamic reduced-order model in this simulation can be expressed as

$$\begin{aligned}
\dot{x_1} &= b_1 + L_{11}x_1 + Q_{141}x_1x_4 + Q_{111}x_1^2 + Q_{121}x_1x_2 \\
&\quad + Q_{131}x_1x_3 + \beta_1\dot{\gamma_1} \qquad (33)\\
\dot{x_2} &= b_2 + [L_{22} + t_2(x_2^2 + x_3^2)]x_2 + L_{23}x_3 \\
&\quad + Q_{212}x_1x_2 + \beta_2\dot{\gamma_2} \qquad (34)\\
\dot{x_3} &= b_3 + L_{32}x_2 + [L_{33} + t3(x_2^2 + x_3^2)]x_3 \\
&\quad + Q_{313}x_1x_3 + Q_{314}x_1x_4 + \beta_3\dot{\gamma_3} \qquad (35)\\
\dot{x_4} &= b_4 + L_{41}x_1 + L_{44}x_4 + Q_{444}x_4^2 \\
&\quad + Q_{414}x_1x_4 + Q_{424}x_2x_4 + Q_{434}x_3x_4 + \beta_4\dot{\gamma_4} \qquad (36)
\end{aligned}$$

with a measurement (i.e., output) equation given by

$$y = \sum_{i=1}^{4} c_i x_i \qquad (37)$$

where x_i is introduced in (2), and c_i, i = 1,...,4 are the weighting coefficients of the output matrix. Without loss of generality, the c_i are assumed to be 1 for the proof of concept in the simulation.

Figures 1 and 2 show the closed-loop response of the states and the control input signals, respectively. These figures show that the adaptive control law achieves zero steady state error in the state regulation, where the non-adaptive has a significant non-zero steady-state error. Based on Figure 2, the commanded control inputs are very large; however, the magnitudes of these actuation values are based on the reduced-order model and do not correspond to physical quantities. It is expected that a more detailed derivation of the numerical values of the input gain terms could result in more reasonable magnitudes of the commanded control inputs, and this is a subject of future work.

To provide an apples-to-apples comparison, the non-adaptive controller is designed with the same structure and control gain values as the adaptive controller, but uses feedforward constant estimates $\hat{\beta}$ of the input-multiplicative parametric uncertainty, which are selected to be equal to the initial conditions of the adaptive parameter estimates $\hat{\beta}(0)$ that are used in the adaptive controller. The non-adaptive controller does not include the feedforward adaptive term $\hat{\theta}_1(t)$.

TABLE I: Initial Conditions of the States and Estimates (Column vectors) (i.e., ';' denotes a new row in the vector)

Parameter	Value
$x(t)$	[2;3;6;2]
$\hat{\theta}_1$	[1673.1; -258.3; 5.4; -20.4; -6.6; -6.9; 3050.7; -1177.2; -7.5; 791.7; 225; 123; -654.9; -22.8; -0.6; 15; 11.7; -1886.7; 130.2; -340.5; -21.9; 8.7; -29.4; 18.9]
$\hat{\theta}_2$	[1;1;1;1]

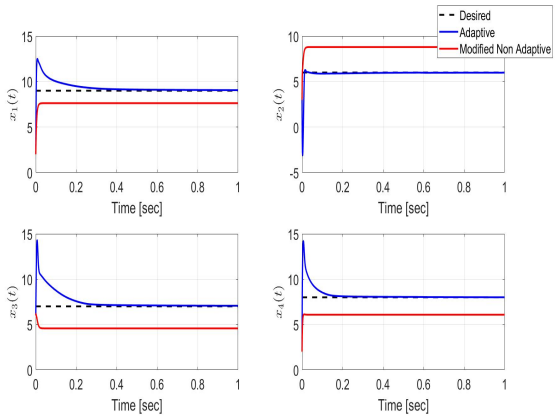

Fig. 1: Closed loop response of the states $x_1(t), x_2(t), x_3(t)$ and $x_4(t)$ with adaptive control (blue solid) and non adaptive controller (red solid) tracking the desired trajectory (black dashed).

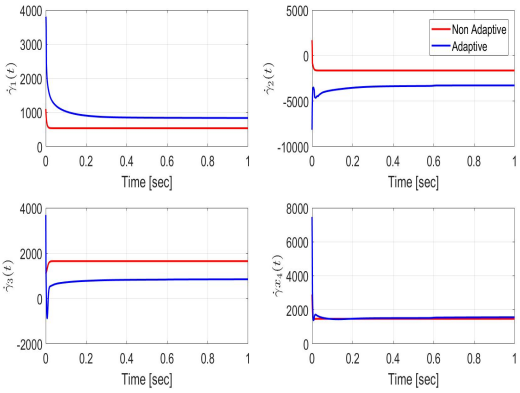

Fig. 2: Closed loop response of the control signal $\dot{\gamma}(t)$ using adaptive control (blue solid) and non adaptive controller (red solid).

VII. Conclusion

A Lyapunov-based adaptive control method is applied to a detailed reduced-order model of the complete actuated dynamics of a fluid flow dynamic system in the presence of parametric uncertainty in the plant model and the actuation model. A rigorous Lyapunov-based stability analysis is utilized to prove that the adaptive control law achieves asymptotic flow field regulation in the presence of the parametric uncertainty. Future work will address 1) a more rigorous derivation of the input gain matrix values in the reduced order model development and 2) methods to quantify the actuation magnitudes in the reduced-order model in physical terms.

Authorized licensed use limited to: Embry-Riddle Aeronautical University. Downloaded on December 27,2022 at 18:13:17 UTC from IEEE Xplore. Restrictions apply.

TABLE II: Parameters Used in the Simulation Plant Model

Linear Terms		Quadratic and Cubic Terms	
$b_1 = 557.7$	$L_{11} = -86.1$	$Q_{111} = 1.8$	$Q_{414} = 2.9$
$b_2 = 1016.9$	$L_{22} = -392.4$	$Q_{121} = -2.2$	$Q_{424} = -9.8$
$b_3 = 41.0$	$L_{23} = 263.9$	$Q_{131} = -2.3$	$Q_{434} = 6.3$
$b_4 = -628.9$	$L_{32} = -218.3$	$Q_{141} = -6.8$	$Q_{444} = -7.3$
	$L_{33} = -7.6$	$Q_{212} = 75.0$	
	$L_{41} = 43.4$	$Q_{313} = 5.0$	$t_2 = -2.5$
	$L_{44} = -113.5$	$Q_{314} = 3.9$	$t_3 = -0.2$

References

[1] A. R. Paul, A. Jain, and F. Alam, "Drag reduction of a passenger car using flow control techniques," *International Journal of Automotive Technology*, vol. 20, no. 2, pp. 397–410, 2019.

[2] C. Prasad and P. Morris, "A study of noise reduction mechanisms of jets with fluid inserts," *Journal of Sound and Vibration*, p. 115331, 2020.

[3] M. DeSalvo, E. Whalen, and A. Glezer, "High-lift performance enhancement using active flow control," *AIAA Journal*, pp. 1–15, 2020.

[4] A. Weingaertner, P. Tewes, and J. C. Little, "Parallel vortex body interaction enabled by active flow control," *Experiments in Fluids*, vol. 61, no. 137, p. 137, 2020.

[5] J. Huang and W.-X. Yao, "Active flow control by a novel combinational active thermal protection for hypersonic vehicles," *Acta Astronautica*, vol. 170, pp. 320–330, 2020.

[6] J. Bons, S. Benton, C. Bernardini, and M. Bloxham, "Active flow control for low-pressure turbines," *AIAA Journal*, vol. 56, no. 7, pp. 2687–2698, 2018.

[7] D. Dolgopyat and A. Seifert, "Active flow control virtual maneuvering system applied to conventional airfoil," *AIAA Journal*, vol. 57, no. 1, pp. 72–89, 2019.

[8] E. A. Whalen, A. Shmilovich, M. Spoor, J. Tran, P. Vijgen, J. C. Lin, and M. Andino, "Flight test of an active flow control enhanced vertical tail," *AIAA Journal*, vol. 56, no. 9, pp. 3393–3398, 2018.

[9] K. B. Kidambi, N. Ramos-Pedroza, W. MacKunis, and S. V. Drakunov, "A closed-loop nonlinear control and sliding mode estimation strategy for fluid flow regulation," *International Journal of Robust and Nonlinear Control*, vol. 29, no. 3, pp. 779–792, 2019.

[10] M. Kiesner and R. King, "Multivariable closed-loop active flow control of a compressor stator cascade," *AIAA Journal*, vol. 55, no. 10, pp. 3371–3380, 2017.

[11] D. Xingya and F. Jianchao, "Closed-loop flow control of an ultra-compact serpentine inlet based on nondimensional model," *Chinese Journal of Aeronautics*, 2020.

[12] B. Choi, Y. Hong, B. Lee, M. Kim, H. J. Kim, and C. Kim, "Adaptive flow separation control over an asymmetric airfoil," *International Journal of Aeronautical and Space Sciences*, vol. 19, no. 2, pp. 305–315, 2018.

[13] V. Motta and L. Malzacher, "Open-loop and closed-loop flow control based on van der pol modeling," *Acta Mechanica*, vol. 229, no. 1, pp. 389–401, 2018.

[14] W. Zou, C. K. Ahn, and Z. Xiang, "Leader-following consensus of second-order nonlinear multi-agent systems with unmodeled dynamics," *Neurocomputing*, vol. 322, pp. 120–129, 2018.

[15] W. Zou, K. Qian, and Z. Xiang, "Fixed-time consensus for a class of heterogeneous nonlinear multiagent systems," *IEEE Transactions on Circuits and Systems II: Express Briefs*, vol. 67, no. 7, pp. 1279–1283, 2019.

[16] Y. Yang, W. Gao, H. Modares, and C. Z. Xu, "Robust actor-critic learning for continuous-time nonlinear systems with unmodeled dynamics," *IEEE Transactions on Fuzzy Systems*, 2019, doi: 10.1109/TFUZZ.2021.3075501.

[17] J. L. Carroll, T. S. Peterson, and N. E. Owens, "Memory-guided exploration in reinforcement learning," in *IJCNN'01. International Joint Conference on Neural Networks. Proceedings (Cat. No. 01CH37222)*, vol. 2, pp. 1002–1007, IEEE, 2001.

[18] S. D. Whitehead, "A complexity analysis of cooperative mechanisms in reinforcement learning.," in *AAAI*, pp. 607–613, 1991.

[19] A. Naruta, T. Mannucci, and E.-J. Van Kampen, "Continuous state and action q-learning framework applied to quadrotor uav control," in *AIAA Scitech 2019 Forum*, p. 0145, 2019.

[20] G. Hardier, G. Ferreres, and M. Sato, "On-line parameter estimation for indirect adaptive flight control: a practical evaluation of several techniques," in *2020 IEEE Conference on Control Technology and Applications (CCTA)*, pp. 180–187, IEEE, 2020.

[21] W. Wei, H. Dourra, and G. G. Zhu, "Deadbeat adaptive backstepping design for tracking transfer case torque and estimating its clutch touchpoint," in *2020 IEEE Conference on Control Technology and Applications (CCTA)*, pp. 188–193, IEEE, 2020.

[22] A. Schwab, L.-M. Reichelt, P. Welz, and J. Lunze, "Experimental evaluation of an adaptive cruise control and cooperative merging concept," in *2020 IEEE Conference on Control Technology and Applications (CCTA)*, pp. 318–325, IEEE, 2020.

[23] G. K. Batchelor, *Turbulence, Coherent Structures, Dynamical System, and Symmetry*. Cambridge, United Kingdom: Cambridge University Press, 2000.

[24] C. Kasnakoğlu, R. C. Camphouse, and A. Serrani, "Reduced-order model-based feedback control of flow over an obstacle using center manifold methods," *Journal of Dynamic Systems, Measurement, and Control*, vol. 131, no. 1, p. 011011, 2009.

Authorized licensed use limited to: Embry-Riddle Aeronautical University. Downloaded on December 27,2022 at 18:13:17 UTC from IEEE Xplore. Restrictions apply.